POLITECNICO DI TORINO
Repository ISTITUZIONALE

Hydrothermal liquefaction of digestate from the organic fraction of municipal solid waste: Optimization of operating parameters

Original
Hydrothermal liquefaction of digestate from the organic fraction of municipal solid waste: Optimization of operating parameters / Tito, E., Landi, D., Demichelis, F., Pipitone, G., Bensaid, S., Pirone, R.. - In: ENERGY CONVERSION AND MANAGEMENT. - ISSN 0196-8904. - 336:(2025). [10.1016/j.enconman.2025.119881]

Availability:
This version is available at: 11583/2999990 since: 2025-05-09T09:22:06Z

Publisher:
Elsevier

Published
DOI:10.1016/j.enconman.2025.119881

Terms of use:

This article is made available under terms and conditions as specified in the corresponding bibliographic description in the repository

Publisher copyright

(Article begins on next page)

24 June 2026

Energy Conversion and Management 336 (2025) 119881

Contents lists available at ScienceDirect

Energy Conversion and Management

journal homepage: www.elsevier.com/locate/enconman

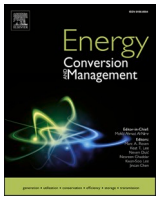

Hydrothermal liquefaction of digestate from the organic fraction of municipal solid waste: Optimization of operating parameters

Edoardo Tito, Daniela Landi, Francesca Demichelis, Giuseppe Pipitone *, Samir Bensaid, Raffaele Pirone

Department of Applied Science and Technology, Politecnico di Torino, Corso Duca degli Abruzzi 24, 10129 Turin, Italy

ARTICLE INFO

Keywords:
Hydrothermal liquefaction
Food waste
Digestate
Biocrude
Solid loading
Waste valorization

ABSTRACT

The growing demand for clean energy and the increasing waste volumes have spurred interest in waste-to-energy processes. Anaerobic digestion (AD) is a well-established technology that converts the organic fraction of municipal solid waste (OFMSW) into biogas, with digestate as a challenging byproduct to manage. This study explored the potential for further valorizing digestate from OFMSW through hydrothermal liquefaction (HTL). A broad range of operating parameters – temperature (300–360 °C), residence time (10–60 min), and dry solid loading (5–30 wt%) – was systematically investigated using a rigorous statistical approach and complementary characterization techniques, leading to new insights on performance indicators. Higher temperatures resulted in a limited residual solid yield (as low as 7 wt%), increased biocrude production (up to 32 wt%) and altered its composition, with an increase in aromatics, a reduction in sterols, and a higher aromatic-to-aliphatic nitrogen ratio. The effect of an increase in dry solid loading on the HTL of digestate, a factor crucial to its economic feasibility, was investigated for the first time. This resulted in higher yields of residual solids (up to 24 wt%) at the expense of aqueous phase soluble compounds and altered the elemental ratios of biocrudes and solids. This study demonstrates that HTL can convert digestate from OFMSW into biocrude, capturing up to 48% of the feedstock's embedded energy in a more concentrated form (~31 MJ/kg), making it a suitable substitute for fossil-derived fuel oil.

1. Introduction

The energy demand is continuously increasing, and in 2023, global primary energy consumption reached 660 EJ/y, with only 23% coming from non-fossil sources [1]. The most significant contributors among these are the traditional use of biomass and hydropower, each accounting for 6% of the total energy share, followed by nuclear at 4% and wind at 3% [1]. In contrast, the three fossil fuels – oil, coal, and natural gas – alone account for 30%, 25%, and 22% of total consumption, respectively, underscoring society's heavy reliance on them [1]. However, fossil fuels are finite resources and will eventually run out. Additionally, their use is a major driver of global warming and rising global temperatures. Given these challenges, it is essential to transition away from fossil fuels by expanding energy production through alternative and renewable sources that are both environmentally and economically sustainable.

Among alternative energy sources, the valorization of waste biomass is attracting increasing interest. Waste biomass encompasses various materials from agricultural and food industries (e.g., straw, manure, bagasse, pomace), households, and industrial activities (e.g., sewage sludge, tall oil, wood). Valorizing waste offers a significant opportunity by combining energy production – either as an energy carrier or through direct energy recovery – with the need to manage growing waste volumes, according to the waste-to-energy paradigm. In particular, the focus on municipal solid waste (MSW) valorization is intensifying, as global MSW is projected to increase from 2.1 Gt/year in 2020 to 3.8 Gt/year by 2050 [2], driven by population growth, economic development, and urbanization [2,3]. Improper landfilling of MSW can contaminate groundwater and soil with heavy metals, organic pollutants, and pathogens [4]. Additionally, between 32 and 57% of the MSW is attributable to its organic fraction (OFMSW, food and green wastes) [5], which poses an environmental concern due to the possible leakages of greenhouse gases like carbon dioxide and methane.

A well-established technology for valorizing OFMSW is wet

* Corresponding author.
E-mail address: giuseppe.pipitone@polito.it (G. Pipitone).

https://doi.org/10.1016/j.enconman.2025.119881
Received 11 December 2024; Received in revised form 19 February 2025; Accepted 28 April 2025
0196-8904/© 2025 The Author(s). Published by Elsevier Ltd. This is an open access article under the CC BY-NC-ND license (http://creativecommons.org/licenses/by-nc-nd/4.0/).

anaerobic digestion (AD) [3]. This process utilizes anaerobic bacteria to break down organic material, converting it into biogas, primarily composed of methane and carbon dioxide. During AD, the organic material is significantly reduced, but 30–65% remains as digestate [6–8]. Digestate is characterized by a high water content (~90 wt%), residual organic matter, and essential mineral nutrients such as nitrogen, sodium, phosphorus, and calcium [9,10]. Due to its nutrient content, digestate could be applied as fertilizer to help close the nutrient cycle [9], and it is considered a chemically not dangerous material [11]. However, proper management is crucial, as excessive application can lead to soil acidification and eutrophication, with harmful effects on both soil and plants [12]. In any case, before being applied as fertilizer, digestate produced through mesophilic AD must be composted for at least 14 days at 55 °C [13]. Moreover, digestate has a very low market value, which could even become negative in certain periods and locations [14]. As a result, alternative methods for valorizing digestate are being explored [15].

Being a highly recalcitrant biomass, digestate could be valorized through thermochemical technologies. In particular, pyrolysis and gasification have garnered attention [16]. However, due to the high moisture content of digestate, an energy-intensive drying step is required before any dry thermochemical process, such as pyrolysis or gasification, resulting in decreased energy efficiency. Valorizing digestate through hydrothermal liquefaction (HTL) offers a way to bypass this step. HTL is a promising technology that allows the conversion of organic substrates into biocrude via reaction in liquid water at medium temperatures (250–374 °C), high pressures (4–25 MPa), and dry solid loading within 5–30 wt% [17–19]. In these operating conditions, water strongly changes its properties favoring the solubilization of organic matter and allowing the breakdown of the complex molecules present therein [20,21]. In this way, it would be possible to convert a fraction of the carbon in the digestate into biocrude, a precursor for producing liquid fuels for the transportation sector, while reducing the amount of digestate requiring disposal.

Some preliminary studies have already investigated the valorization of digestate through HTL. Specifically, they studied the valorization of digestate from sewage sludge [22–30], and from manure [31–34]. However, to the best of the authors' knowledge, only Klüpfel et al. have evaluated the HTL of digestate derived from the biogenic fraction of urban solid waste [35,36]. In their study, KOH was used as a homogeneous catalyst, and the dry solid loading was maintained fixed at 16.6 wt % [35]. KOH was used because it is known to enhance biocrude production during HTL [37]. However, its presence could be detrimental if the post-HTL aqueous phase (AP) is recycled for diluting the organic fraction before anaerobic digestion (AD), as reducing water demand in the overall process would necessitate this step. The optimal pH range for AD is within 6.7–7.5 [38], and KOH could raise it beyond this range.

Another knowledge gap concerns the effect of dry solid loading on the performance of HTL of digestate. To the best of the author's knowledge, this effect has never been studied for digestate derived from OFMSW or any other type of digestate. Due to the low total solids in digestate, concentrating solids is necessary, albeit challenging [15], and this step generates a liquid fraction alongside the solid digestate, which requires disposal [39,40]. Processing diluted digestate in HTL could reduce liquid fraction disposal by lowering organic content, but it would increase HTL costs, as dry solid loading has been observed to affect the profitability of the HTL process strongly [41,42]. Studying the scientific effects of solid loading on HTL performance, both qualitatively and quantitatively, is essential for identifying the optimal conditions that facilitate efficient AD-HTL coupling.

This study aimed to address this knowledge gap by evaluating the performance of HTL on solid digestate from OFMSW without catalyst by varying key operating parameters over a wide range, following a design of experiment approach: temperature (300–360 °C), residence time (10–60 min), and dry solid loading (5–30 wt%). Temperature and reaction time were selected as they are the most studied variables in subcritical HTL, with the chosen ranges covering typical process conditions. Dry solid loading was also examined as it impacts overall AD-HTL process performance. Its investigated range was designed to include values representing both raw digestate (5 wt%) and highly concentrated solid digestate obtained through centrifugation and filter pressing (30 wt%). The different phases produced during HTL – biocrude, solid, gas, and aqueous phase – were quantified and thoroughly analyzed. Gaining a deeper understanding of HTL's performance on OFMSW digestate, this work lays the foundations for enabling a more effective optimization of the HTL-AD integration.

2. Materials and methods

2.1. Materials

Experiments were performed using digestate obtained from anaerobic digestion (mesophilic at 37 °C and 8 wt% of total solid feed) in a waste treatment plant that processes the organic fraction of municipal solid wastes (OFMSW) and green waste in Pinerolo, Italy. Before transportation, the digestate was concentrated into a solid form using a filter press. The properties of the received solid digestate are reported in Table 1. After reception, the digestate was stored wet in a refrigerator and then used in the experimental tests. Distilled water was used to dilute the digestate, while diethyl ether (Reag. Ph Eur, 1.00921, Supelco) and acetone (>99.5% GC, 32201-M, Sigma-Aldrich) were used as post-reaction solvents.

2.2. Design of experiment (DoE)

Experiments were conducted by varying three operating variables: temperature, residence time, and dry solid loading. The experimental campaign was defined via a design of experiment (DoE) approach, based on three factors and three levels for each (Table 2). The chosen design was a Box-Bhenken design (green and blue dots in Fig. 1), supplemented by the factorial points (orange dots in Fig. 1). The central point was tested five times, while all other points were tested twice.

Multiple linear regression was used to determine the coefficients (β_i) of the general quadratic equation (Eq. (1)) for each variable, providing a better approximation of the experimental results. In Eq. (1), T represents temperature, t denotes residence time, and SL corresponds to dry solid loading, expressed in either coded (−1, 0, 1) or uncoded (°C, min, wt%) form. Key statistical parameters were analyzed alongside an analysis of

Table 1
Digestate properties.

Proximate analysis	
Moisture content (wt% *wb*)	57.2 ± 0.7
Ash (wt% *db*)	42.0 ± 0.2
Ultimate analysis (wt% *daf*)	
Carbon	50.5 ± 0.3
Hydrogen	5.8 ± 0.2
Nitrogen	4.9 ± 0.1
Sulfur	1.7 ± 0.5
Oxygen*	37.1 ± 1.4
Biochemical composition (wt% *daf*)	
Lignin	44.8 ± 1.5
Protein	30.4 ± 0.9
Carbohydrates	21.9 ± 3.1
Lipids	3.0 ± 0.6
Solubility test (wt% *daf*)**	
Solid	78.8 ± 3.0
Biocrude	5.4 ± 0.5
Aqueous phase*	15.8 ± 3.5

*Evaluated by difference; **performed with a dry solid concentration of 5 wt%.

Table 2
Factors and levels used in the DoE.

Factor	Levels		
	−1	0	1
Temperature (°C)	300	330	360
Residence time (min)	10	35	60
Dry solid loading (wt%)	5	17.5	30

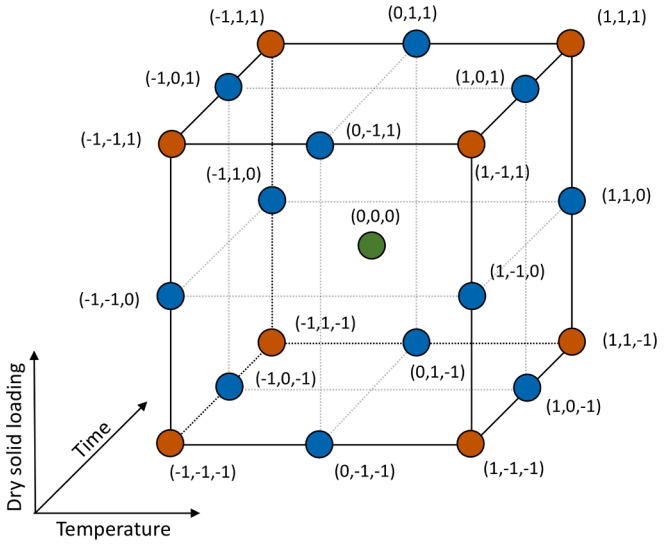

Fig. 1. Modified Box-Behnken design with factorial points applied in this work.

variance (ANOVA) to assess the regression's goodness of fit. The resulting equations for each variable were then visualized within the design space (temperature, time, and solid loading) to generate response surfaces and contour maps.

$$Variable = \beta_0 + \beta_T T + \beta_t t + \beta_{SL} SL + \beta_{Tt} Tt + \beta_{TSL} TSL + \beta_{tSL} tSL + \beta_{T^2} T^2 + \beta_{t^2} t^2 + \beta_{SL^2} SL^2 \quad (1)$$

2.3. Reaction procedure

Experiments were performed in 20 mL bomb-type reactors constructed from a 3/4″ 316 stainless steel tube, with both ends sealed by caps. Before starting the reaction, the reactors were loaded with wet digestate and distilled water to obtain the desired dry solid loading and a total slurry mass of 9 g. After loading, the reactors were submerged into a sand bath (Techne© SBL-2D, controller Techne© TC-9D) preheated to the set-point temperature. Within 190–220 s, the temperature inside the reactor reached 95% of the temperature change between 25 °C and set-point temperature [43] – 287, 315, or 343 °C, depending on the experimental conditions, resulting in a heating rate within 83–93 K/min. After reaching that temperature (squares in the temperature profile reported in Fig. S1), the desired operating time was maintained before removing the reactors from the sand bath and placing them in water for 5 min. Within less than 50 s the internal temperature dropped below 50 °C.

2.4. Post-reaction work-up

After cooling, the reactors were dried with compressed air, weighed, opened to vent the produced gas, and weighed again. The difference between the two weights provided the mass of gas produced. Subsequently, the reactor contents were poured into a 50 mL falcon tube along with 35 mL of diethyl ether previously added to the reactor to help collect any residues present. Using a spatula, additional residual solids were transferred to the falcon tube, which was then mixed with a vibromixer for a few seconds and centrifuged at 5000 rpm for 10 min. Three phases were separated: a supernatant apolar phase, an aqueous phase, and a sedimented solid. The apolar phase was collected with a Pasteur pipette and vacuum filtered with a Büchner filter. The aqueous phase was also vacuum filtered, collected in an Eppendorf tube, and stored in the fridge. The solid left in the 50 mL falcon tube was put in contact with acetone, which was then filtered using the same filter containing solid traces from the aqueous and diethyl ether phases. All the solid was transferred to the filter, and acetone was added until the permeate was colorless. The filter containing all the solids was placed in an oven at 105 °C overnight and then weighed to determine the mass of the solid. The apolar phase, consisting of both diethyl ether and acetone phases, was transferred to a 50 mL round-bottom flask and subjected to distillation using a rotary evaporator. The residual biocrude was then redissolved in diethyl ether, dried with sodium sulfate, filtered, and rotary evaporated again to obtain the resulting dried biocrude. Solid and biocrude samples were collected and stored until needed for analysis.

2.5. Analysis

To assess the biochemical content of the digestate, moisture, lipids, proteins, lignin, and ashes were measured, while carbohydrates were calculated by difference. The moisture content was measured as the mass removed after drying overnight in an oven at 105 °C. The protein content was calculated by multiplying the nitrogen content, which was evaluated through elemental analysis, by a factor of 6.25 [44]. The lipid content was determined by Soxhlet extraction of 5 g of dry digestate with 200 mL of petroleum ether heated to 70 °C for 6 h. The extracted material was then subjected to evaporation by a rotary evaporator to remove the petroleum ether, and the remaining mass was accounted for as lipids. The lignin content was quantified as the acid-insoluble ('Klason') lignin defined by the TAPPI standard [45].

The mass yields of the different phases were calculated on a dry and ash-free basis (*daf*), according to Eq. (2). The aqueous phase (AP) yield was evaluated as the difference from 100% of the yields of the other phases (Eq. (3)). An elemental analyzer (Elementar vario Macro Cube) was used to determine the elemental composition (CHNS) of feedstock, biocrude, aqueous, and solid phases. The ashes of the digestate were measured as the residue left after combustion in an oven at 550 °C for 6 h. The ashes in the produced solids were evaluated via thermogravimetric analysis (TGA, Mettler Toledo SDTA851). The organic carbon content in the solids and the digestate was determined by subtracting the carbon-equivalent associated with CO_2 release from carbonates (measured between 550 and 900 °C via TGA) from the total carbon measured by the elemental analyzer.

Higher heating values (HHVs) for solid and biocrude phases were evaluated from the elemental analysis, according to the work from Channiwala & Parikh [46]. The carbon/nitrogen yield of the phases was calculated by dividing the masses of organic carbon/nitrogen in the phases by the organic carbon/nitrogen content of the feedstock (Eq. (4) and Eq. (5)). Energy recovery (ER) was calculated according to Eq. (6), where HHV values are given in MJ/kg. The net energy recovery (NER) was calculated to preliminarily evaluate energy profitability. The calculation accounted for the heating demand of the wet digestate, as reported in Eq. (7). Due to heat integration, it was assumed that only the final 35 °C needed to be supplied to reach the set-point temperature [47]. The heat capacity of the wet digestate was assumed to be equivalent to that of water within the required temperature range [41].

The compositions of biocrude, and aqueous samples were analyzed using a GC (Agilent 7890A GC) coupled with MS (Agilent 5975C). Samples of biocrude were diluted 1:100 v/v in acetone. 1 μL of diluted sample was injected on a DB-5 ms column (dimensions 30 m × 0.25 mm × 0.25 μm) in split mode with a split ratio 20:1, injection temperature of 280 °C. The helium flow in the column was kept constant at 1 mL/min while the temperature programming was 40 °C (5 min soak)//10 °C/

min//100 °C (0 min soak)//4 °C/min//280 °C (0 min soak)//10 °C/min//300 °C (0 min soak). The identification of compounds was based on NIST 17 library and only compounds with a match factor greater than 70 and a peak area greater than 1% of the largest peak were considered.

The aqueous samples were derivatized with methyl chloroformate (MCF) according to the technique analysis developed by Madsen et al. [48]. A 200 µL aqueous sample was added to a 2 mL vial, followed by 40 µL of NaOH solution (5 wt%) and 40 µL of pyridine. Then, 20 µL of MCF was added to the solution twice (2 × 20 µL), with vortexing after each addition. The derivatized molecules were extracted and transferred into 400 µL of chloroform containing an internal standard (20 µg/mL of 4-bromotoluene), favored by the addition of 400 µL of $NaHCO_3$ (50 mM). Once the chloroform phase was transferred to a clean vial, 1 µL of sample was injected on a DB-5 ms column (dimensions 30 m × 0.25 mm × 0.25 µm) in split mode with a split ratio 20:1, injection temperature of 280 °C. The helium flow in the column was kept constant at 0.8 mL/min while the temperature programming was 40 °C (1 min soak)//5 °C/min//300 °C (5 min soak).

To analyze the gas phase, a slight modification to the reactor configuration was made, as described in a previous work [43]. After loading the slurry, and before the reaction step, the reactor was purged with He and then pressurized to 3 bar with He. After the reaction, a gas sample was collected with a syringe and injected into a Micro-GC (SRA) equipped with Molsieve 5A and PoraPLOT U columns, and a TCD detector. Quantification of the gas phase was based on the final concentration of He (used as the internal standard), according to the ideal gas law. Additionally, 300 µL of gas phase was injected into the GC–MS, similar to the procedure described in the literature [49]. A DB-5 ms column (dimensions 30 m × 0.25 mm × 0.25 µm) was used in split mode with a split ratio 25:1, an injection temperature of 150 °C, MS in scan mode from 30 to 300 *m/z*, with a source temperature of 250 °C and quadrupole temperature of 150 °C. The helium flow in the column was kept constant at 1 mL/min while the temperature programming was 40 °C (8 min soak)//20 °C/min//240 °C (1 min soak). The identification of compounds was performed analogously to the protocol used for the biocrude.

$$Mass\ yield_{product,daf}(\%) = \frac{mass_{product,daf}}{mass_{feedstock,daf}} \tag{2}$$

$$AP\ yield_{daf}(\%) = 1 - biocrude\ yield_{daf}(\%) - solid\ yield_{daf}(\%) - gas\ yield_{daf}(\%) \tag{3}$$

$$Carbon\ yield_{product}(\%) = mass\ yield_{product,daf} \cdot \frac{organic\ carbon\ in\ product_{\%daf}}{organic\ carbon\ in\ feedstock_{\%daf}} \tag{4}$$

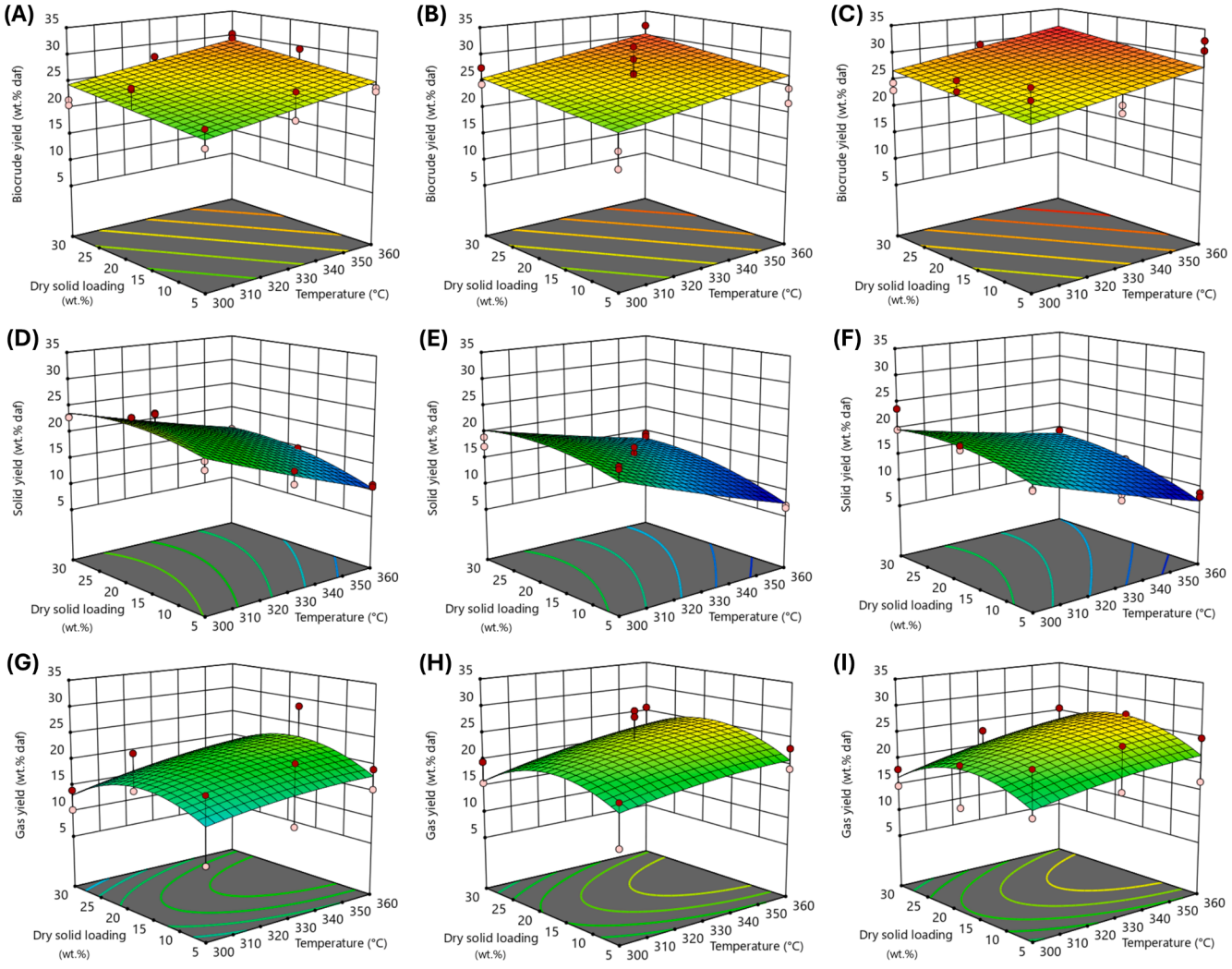

Fig. 2. Response surfaces for the mass yields (wt% daf) obtained from HTL of digestate. Biocrude mass yields after residence times of 10 min (A), 35 min (B), and 60 min (C). Solid mass yields after residence times of 10 min (D), 35 min (E), and 60 min (F). Gas mass yields after residence times of 10 min (G), 35 min (H), and 60 min (I).

$$Nitrogen\ yield_{product}(\%) = mass\ yield_{product,daf} \cdot \frac{nitrogen\ in\ product_{\%daf}}{nitrogen\ in\ feedstock_{\%daf}} \quad (5)$$

$$ER(\%) = \frac{mass_{product,dry}}{mass_{feedstock,dry}} \cdot \frac{HHV_{product,dry}}{HHV_{feedstock,dry}} \quad (6)$$

$$NER(\%) = \frac{HHV_{biocrude}\left(\frac{MJ}{kg_{biocrude}}\right)}{heating\ energy\left(\frac{MJ}{kg_{wet\ \ digestate}}\right)} \cdot biocrude\ yield\left(\frac{kg_{biocrude}}{kg_{wet\ \ digestate}}\right) \quad (7)$$

3. Results and discussion

3.1. Mass yields

The contour plots for the mass yields are shown in Fig. 2, with red/pink dots representing the experimental results obtained, which are reported for clarity in Supplementary Table S1. The contour plots graphically depict the predictive models obtained through regression of the experimental data. The resulting equations for biocrude, solid, and gas are given in their uncoded form as Eq. (8), Eq. Eq. (9), and Eq. (10), respectively. Temperature (T) is expressed in °C, residence time (t) is expressed in min, while dry solid loading (SL) is expressed in wt%. The coded form of these equations is reported in the Supplementary Material as Eqs. (S1)-(S3), while the analysis of variance (ANOVA) is shown in Tables S2-S4, indicating that all the models were statistically significant. Further diagnostic graphs (Figs. S2–S4) were plotted to estimate the predictability of the models.

$$Biocrude\ yield_{(wt\%)} = -3.97 + 7.96{\cdot}10^{-2}T + 4.59{\cdot}10^{-2}t + 1.34{\cdot}10^{-1}SL \quad (8)$$

$$\begin{aligned} Solid\ yield_{(wt\%)} = {} & 1.13{\cdot}10^{2} - 3.79{\cdot}10^{-1}T - 4.36{\cdot}10^{-1}t - 3.57{\cdot}10^{-1}SL \\ & + 6.00{\cdot}10^{-4}Tt + 2.51{\cdot}10^{-3}TSL + 8.80{\cdot}10^{-4}tSL \\ & + 2.55{\cdot}10^{-4}T^{2} + 2.17{\cdot}10^{-3}t^{2} - 9.73{\cdot}10^{-3}SL^{2} \end{aligned} \quad (9)$$

$$\begin{aligned} Gas\ yield_{(wt\%)} = {} & -8.58{\cdot}10^{1} + 5.56{\cdot}10^{-1}T + 6.16{\cdot}10^{-1}t + 2.90{\cdot}10^{-1}SL \\ & + 3.78{\cdot}10^{-4}Tt + 1.87{\cdot}10^{-3}TSL + 5.73{\cdot}10^{-4}tSL \\ & - 7.91{\cdot}10^{-4}T^{2} - 1.80{\cdot}10^{-3}t^{2} - 2.67{\cdot}10^{-2}SL^{2} \end{aligned} \quad (10)$$

The results obtained for the biocrude yield showed little variations across the entire operating range studied (Figs. 2A-B-C). The extreme values predicted by the model were 21.0 ± 3.2 wt% at 300 °C for 10 min and 5 wt% solids, and 31.5 ± 3.2 wt% at 360 °C for 60 min and 30 wt% solids. Only 3.0 $wt\%_{daf}$ of lipids were present in the digestate, and lipids are well known for significantly contributing to biocrude production [50,51], due to their already oil-like nature. For this reason, it is worth noting that biocrude was produced from the conversion of the other biochemical families. Interestingly, the best-fitting equation for expressing the biocrude yield followed a linear model (Eq. (8)). From the analysis of variance (Table S2, Eq. (S1)), the most significant and impactful operating condition was temperature, which led to a slight increase in biocrude yield. Water strongly changes its properties in a hydrothermal environment with temperature variation [52], hence, it is expected that temperature has the most significant impact on HTL performance. However, despite the broad range of temperatures considered in this work, from subcritical (300 °C) up to near-critical conditions (360 °C), the differences in biocrude production were not particularly high. In contrast, the chemical composition differences were more pronounced, as discussed in Section 3.4.2. Increasing the dry solid loading also enhanced biocrude production, though to a lesser degree than temperature, while extending the residence time from 5 to 60 min resulted in only minimal increases. The trend with temperature was similar to that observed by Klüpfel et al. after HTL of digested biogenic waste, although they reported a plateau with increasing residence time [35]. Furthermore, the biocrude mass yields obtained in this study were relatively higher than those reported by Klüpfel et al. [35], likely due to differences in the biochemical composition of the starting digestate. The digestate used in this study contained more protein and lignin and fewer carbohydrates, which may have contributed to the increased yield.

The contour plot for the solid yield showed lower values than that for the biocrude yield (Figs. 2D-E-F). The highest amounts of solid were obtained with the lowest temperature (300 °C) and the shortest residence time (10 min), resulting in yields of 22–24 wt%. However, it must be noted that the amounts of residual solid were higher than those expressed on a dry and ash-free basis, as a high quantity of the starting feedstock consisted of ashes (42 $wt\%_{db}$, Table 1). The ash content in the residual solid was between 69–88$\%_{db}$, according to the operating conditions tested, meaning that 61–99% of the starting ashes were retained in the solid phase. For this reason, when expressed on a dry basis, the solid yield at 300 °C and 10 min was experimentally evaluated to be within 45–50 $wt\%_{db}$.

Increasing the temperature had the most significant effect on reducing solid yield, followed by increasing the residence time and decreasing the solid loading. A similar trend with temperature and time was observed by Klüpfel et al. after HTL of digested biogenic waste [35]. This can be attributed to the fact that converting such a recalcitrant feedstock requires sufficiently high temperatures, an appropriate water-to-solid ratio, and ample reaction time. Indeed, near-critical state conditions enhance water reactivity, while a higher water-to-solid ratio provides more water molecules to react with or solubilize the feedstock. The predicted solid yield at the highest temperature (360 °C) and lowest dry solid loading (5 wt%) tested was minimal, ranging from 7-10 wt%, representing the optimal condition.

Regarding the gas phase (Figs. 2G-H-I), the resulting model (Eq. (10)) was less able to explain the difference observed under various operating conditions. The cause can be attributed to the limited variations in the gas phase within the experimental domain tested and the consistent experimental errors in its measurement. According to the model, a minimum of 13.0 ± 4.3 wt% can be obtained at 300 °C for 10 min at 30 wt% solids, while a maximum of 26.6 ± 4.3 wt% can be obtained at 360 °C for 60 min at 19 wt% solids. Increases in temperature and residence time led to higher gas yields, with temperature having a more significant impact. Higher temperatures favor cracking reactions, which result in increased gas production [53–56]. Additionally, as gas is an end-product of HTL rather than an intermediate, its yield either increases or reaches a plateau with increased residence times [54]. Interestingly, solid loading substantially impacted the gas yield according to a negative quadratic order, resulting in a maximum yield with an intermediate solid loading. A similar behavior was observed by Singh et al. after increasing the dry solid loading from 8 to 14 and 25 wt% for the HTL of water hyacinth [57]. Conversely, other studies indicated that increasing solid loading led to higher gas yields, although the maximum solid loadings tested in those studies ranged from 14 to 17 wt% [58–60]. In this work, similar to the experiments conducted by Singh et al. [57], substantially higher values of dry solid loading were tested (25 wt% and 30 wt%). Consequently, the gas yield is likely constrained by lower solid conversion rates above a certain level of dry solid loading due to reduced water availability.

Given that increasing temperature and residence time both influenced the mass yields of all phases in a similar increasing/decreasing trend, and considering that temperature had a greater impact than residence time, these two variables can be combined into the kinetic severity factor (KSF, Eq. (11)), as previously speculated [43,61]. T(t) denotes the temperature (°C) at time t (min); t_0 corresponds to the starting time, while t_f represents the ending time of the reaction. The KSF was calculated for each reaction according to the temperature

profiles in Fig. S1, and the mass yields for all phases are shown in Fig. S5 as a function of KSF. It can be observed that, with solid loading kept constant, the biocrude and gas yields increased slightly with increasing KSF, while the solid yield decreased significantly, following a linear trend.

$$KSF = log_{10}(R^0) = log_{10}\left(\int_{t_0}^{t_f} e^{\frac{T_{(t)}-100}{14.75}} dt\right) \quad (11)$$

3.2. Elemental analysis

The elemental compositions of all biocrudes and solids produced are reported in Table 3, while the concentrations of carbon and nitrogen in the aqueous phase are provided in Table S5. The carbon content of the biocrudes increased from 50 $wt\%_{daf}$ (Table 1) in the starting digestate to 65–74 $wt\%_{daf}$, while the oxygen content decreased from 37 $wt\%_{daf}$ to 12–26 $wt\%_{daf}$, and the nitrogen content expanded from 4.9 $wt\%_{daf}$ in digestate to 2.4–6.2 $wt\%_{daf}$. Fig. 3 shows the van Krevelen diagrams for all biocrude samples, indicating that under all operating conditions, the elemental O/C ratio was reduced to less than half that of the digestate (Fig. 3A), while the H/C ratio decreased slightly. This change could be explained by the occurrence of a combination of dehydration and decarboxylation reactions, among others, as suggested by the arrows in Fig. 3. Regarding the elemental N/C ratio (Fig. 3B), there was a much greater variation, ranging from 0.04 to 0.12 compared to the initial 0.09 in the digestate. Increases in the N/C ratio can likely be attributed to decarboxylation, while decreases may result from deamination. Additionally, due to the lower abundance of nitrogen atoms compared to oxygen, the impact of deamination reactions would be almost imperceptible in Fig. 3A.

Interestingly, subtle trends in the elemental ratios were observed with changes in solid loading rather than temperature, despite temperature being the primary factor influencing biocrude yield. Specifically, lower dry solid loading led to reduced H/C, while the N/C ratio peaked at intermediate solid loadings. These trends were statistically significant and the analysis of variance is reported in Table S6-S7, while the resulting equations are provided in Eq. (S4) and Eq. (S5). A possible explanation for the N/C trend is described in Section 3.3, while the H/C trend, also observed by Motavaf & Savage [62], could be due to the formation of molecules with a higher H/C ratio at higher solid loadings, which simultaneously increase biocrude production.

Because of the increased carbon and decreased heteroatom content, along with the absence of a substantial amount of ashes, the HHVs (Table 3) of the biocrudes increased enormously (27–33 MJ/kg_{db}) compared to that of the digestate (11 MJ/kg_{db}). However, no statistically significant differences were observed with variations in operating

Table 3
Elemental compositions, HHVs and ERs for biocrudes and solids.

Run	Biocrudes							Solids						
	Elemental composition (wt% *daf*)					HHV (MJ/kg *db*)	ER (%)	Elemental composition (wt% *daf*)					HHV (MJ/kg *db*)	ER (%)
	C	H	N	S	O*			C	H	N	S	O		
300 °C-10 min-5%	73.9 ± 2.9	7.6 ± 0.1	2.4 ± 0.0	0.8 ± 0.2	13.7 ± 3.2	33.4 ± 1.5	36.8 ± 2.4	67.2 ± 2.8	5.4 ± 0.5	3.0 ± 0.1	2.8 ± 0.2	21.7 ± 3.1	5.7 ± 0.6	22.8 ± 3.5
300 °C-35 min-5%	73.2 ± 2.5	6.8 ± 0.4	4.0 ± 1.7	1.4 ± 0.8	12.7 ± 2.0	32.4 ± 1.2	27.8 ± 1.0	63.2 ± 4.9	4.6 ± 0.7	2.7 ± 0.2	1.8 ± 0.1	27.6 ± 3.3	5.0 ± 0.9	19.0 ± 4.5
300 °C-60 min-5%	72.3 ± 2.5	7.8 ± 0.1	3.5 ± 0.5	0.9 ± 0.1	13.1 ± 2.2	33.1 ± 1.2	48.8 ± 0.7	72.3 ± 0.8	6.0 ± 0.0	3.2 ± 0.0	2.9 ± 0.1	15.6 ± 0.7	4.9 ± 0.1	18.8 ± 0.5
300 °C-10 min-17.5%	70.2 ± 6.6	7.2 ± 0.4	6.1 ± 0.6	0.7 ± 0.2	12.0 ± 6.5	31.7 ± 3.4	43.8 ± 5.1	61.9 ± 3.6	4.0 ± 1.4	3.1 ± 0.5	2.2 ± 0.2	28.8 ± 6.8	6.1 ± 0.3	26.7 ± 1.4
300 °C-60 min-17.5%	68.4 ± 0.0	7.0 ± 0.1	5.2 ± 0.7	0.7 ± 0.1	15.4 ± 0.5	30.6 ± 0.1	42.5 ± 2.3	73.3 ± 0.3	4.9 ± 0.0	3.9 ± 0.1	2.3 ± 0.0	15.7 ± 0.3	5.4 ± 0.0	22.6 ± 0.4
300 °C-10 min-30%	68.0 ± 2.1	7.7 ± 0.1	3.6 ± 0.6	0.4 ± 0.1	17.8 ± 1.3	30.9 ± 0.8	33.8 ± 0.3	71.5 ± 2.8	5.4 ± 0.5	4.5 ± 0.0	2.3 ± 0.6	16.3 ± 3.5	6.1 ± 0.6	27.5 ± 2.5
300 °C-35 min-30%	67.8 ± 1.1	7.3 ± 2.6	5.2 ± 0.7	0.8 ± 0.8	16.4 ± 2.8	30.9 ± 2.1	43.1 ± 5.0	84.0 ± 1.8	6.0 ± 0.1	4.9 ± 0.1	2.9 ± 0.1	2.2 ± 1.8	5.7 ± 0.2	22.3 ± 4.9
300 °C-60 min-30%	68.2 ± 2.9	7.8 ± 0.2	4.5 ± 0.2	0.7 ± 0.0	15.8 ± 3.4	31.4 ± 1.6	38.8 ± 3.7	72.2 ± 1.2	4.7 ± 0.1	4.4 ± 0.2	2.2 ± 0.2	16.6 ± 1.3	5.7 ± 0.2	23.6 ± 1.8
330 °C-10 min-5%	70.9 ± 2.3	7.0 ± 0.6	3.2 ± 0.7	1.5 ± 1.2	15.2 ± 2.3	31.5 ± 1.2	40.1 ± 5.1	72.1 ± 2.1	5.4 ± 0.6	2.7 ± 0.0	1.8 ± 0.5	18.1 ± 2.8	6.1 ± 0.4	19.7 ± 2.9
330 °C-60 min-5%	70.0 ± 0.2	6.7 ± 0.2	3.1 ± 1.1	1.2 ± 0.1	16.9 ± 1.3	30.6 ± 0.4	36.9 ± 1.1	68.9 ± 2.7	4.7 ± 0.2	2.5 ± 0.2	2.1 ± 0.5	21.7 ± 2.7	3.2 ± 0.3	10.7 ± 0.8
330 °C-35 min-17.5%	71.0 ± 2.3	7.6 ± 0.8	4.5 ± 1.4	0.7 ± 0.1	14.0 ± 1.9	32.4 ± 1.8	46.7 ± 5.4	73.5 ± 8.6	5.1 ± 0.8	3.2 ± 0.2	2.2 ± 0.2	16.0 ± 9.5	4.4 ± 1.2	18.3 ± 6.3
330 °C-10 min-30%	67.6 ± 3.6	7.2 ± 0.9	3.0 ± 0.8	0.7 ± 0.2	19.4 ± 5.0	30.1 ± 2.7	42.3 ± 5.4	80.2 ± 7.0	5.8 ± 1.0	4.1 ± 0.1	2.6 ± 0.0	7.4 ± 8.5	5.8 ± 1.2	12.6 ± 2.7
330 °C-60 min-30%	68.1 ± 4.3	7.6 ± 0.7	6.2 ± 2.4	0.7 ± 0.2	14.8 ± 2.6	31.1 ± 2.4	46.1 ± 2.9	77.3 ± 3.1	4.8 ± 0.2	4.1 ± 0.2	2.5 ± 0.0	11.3 ± 3.5	4.6 ± 0.4	18.7 ± 1.7
360 °C-10 min-5%	71.0 ± 0.4	7.5 ± 0.2	3.0 ± 0.5	1.1 ± 0.4	15.5 ± 0.1	32.1 ± 0.1	40.7 ± 1.0	69.5 ± 4.9	5.6 ± 0.3	2.6 ± 0.1	3.3 ± 1.2	19.0 ± 6.3	3.0 ± 0.6	9.9 ± 1.7
360 °C-35 min-5%	70.0 ± 1.6	6.7 ± 0.5	4.5 ± 0.6	1.0 ± 0.1	14.9 ± 2.6	30.8 ± 1.4	37.1 ± 1.3	87.1 ± 4.7	6.3 ± 0.4	2.9 ± 0.0	1.8 ± 0.2	1.9 ± 5.2	2.8 ± 0.4	8.3 ± 1.4
360 °C-60 min-5%	65.4 ± 3.3	7.4 ± 0.0	3.1 ± 0.5	0.7 ± 0.1	21.2 ± 4.0	29.4 ± 1.6	49.1 ± 4.7	75.7 ± 0.3	5.2 ± 0.0	2.6 ± 0.1	1.6 ± 0.3	15.0 ± 0.5	2.0 ± 0.0	6.7 ± 0.5
360 °C-10 min-17.5%	66.4 ± 10.8	7.3 ± 0.2	5.6 ± 0.4	0.7 ± 0.2	16.4 ± 11.6	30.1 ± 5.2	48.2 ± 2.4	69.3 ± 4.0	4.6 ± 0.2	3.2 ± 0.2	2.3 ± 0.1	20.6 ± 4.2	3.0 ± 0.5	11.1 ± 1.7
360 °C-60 min-17.5%	65.5 ± 0.6	7.0 ± 0.1	5.5 ± 0.5	0.7 ± 0.0	17.7 ± 1.2	29.3 ± 0.5	41.7 ± 3.5	72.1 ± 2.7	4.5 ± 0.4	3.1 ± 0.1	1.4 ± 0.2	18.9 ± 3.2	2.7 ± 0.4	9.8 ± 1.3
360 °C-10 min-30%	67.8 ± 2.0	7.8 ± 0.1	4.2 ± 0.0	0.4 ± 0.0	17.0 ± 2.1	31.1 ± 1.1	48.4 ± 2.6	66.8 ± 1.6	5.2 ± 0.3	3.5 ± 0.1	2.7 ± 0.0	21.9 ± 2.2	3.7 ± 0.3	14.1 ± 1.0
360 °C-35 min-30%	71.1 ± 1.8	8.0 ± 0.2	4.6 ± 1.2	0.4 ± 0.0	13.1 ± 2.7	32.8 ± 1.1	53.1 ± 9.3	81.7 ± 1.4	4.8 ± 0.2	4.1 ± 0.1	2.7 ± 0.0	6.7 ± 1.5	3.8 ± 0.1	16.8 ± 0.7
360 °C-60 min-30%	60.4 ± 1.0	7.1 ± 0.2	3.7 ± 1.2	0.5 ± 0.0	25.9 ± 2.4	26.7 ± 0.9	42.2 ± 1.4	71.9 ± 2.4	4.0 ± 0.2	3.4 ± 0.2	1.5 ± 0.1	19.1 ± 2.7	2.8 ± 0.3	10.9 ± 1.1

*Evaluated by difference.

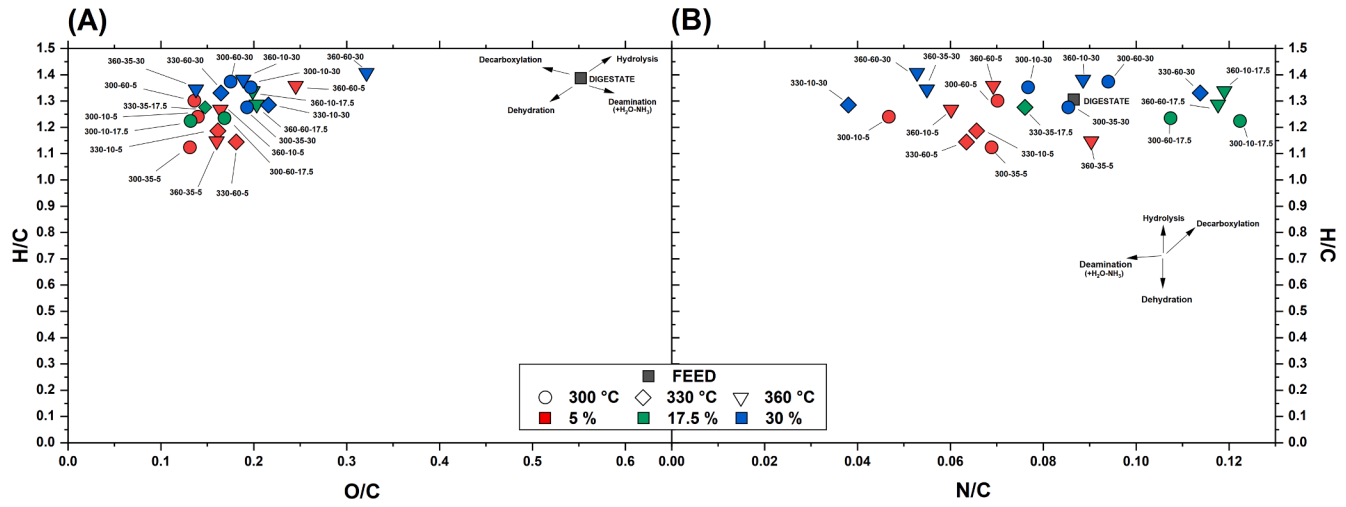

Fig. 3. Van Krevelen diagrams for biocrudes. (A) H/C vs O/C; (B) H/C vs N/C. Labels indicate temperature(°C)-time(min)-dry solid loading(wt%) of the sample. Symbol shapes represent temperature, while colors indicate dry solid loading, as shown in the legend.

parameters. Moreover, a substantial amount of the energy embedded in the digestate was transferred to the biocrudes, as the experimentally evaluated energy recoveries (ERs, Table 3) for biocrudes were within 28–53%. By modeling the behavior of energy recovery (Fig. S6), slight increases were observed with increased temperature and dry solid loading. This was attributed to increased biocrude production rather than changes in the energy density of the biocrude. From Fig. S6, the highest ER was equal to 48% at 360 °C, 60 min and 30 wt%.

The O/C ratios obtained in this work were lower, and the HHVs were higher than those typically achieved through pyrolysis [63–65]. For instance, Monlau et al. performed pyrolysis at 500 °C of digestate obtaining a biocrude having an O/C ratio of 0.45 and an HHV of 23.5 MJ/kg [65], which are roughly double and considerably lower, respectively, than those found in this study. Therefore, beyond the benefit of processing digestate in its wet state, HTL offers the significant advantage of producing a biocrude with superior properties compared to pyrolysis.

Regarding the solid phase (Table 3), the carbon concentration increased substantially compared to that of the digestate (50 $wt\%_{daf}$), with carbon values ranging from 62 to 87 $wt\%_{daf}$. Conversely, nitrogen decreased from 4.9 wt% to a range of 2.5–4.9 $wt\%_{daf}$, while hydrogen varied from 5.8 $wt\%_{daf}$ to 4.0–6.3 $wt\%_{daf}$. It is worth noting that these concentrations are expressed on a *daf* basis, and that on a dry basis the concentrations of carbon, hydrogen, nitrogen, sulfur, and oxygen decreased in all cases. Due to the high ash concentration (69–88$\%_{db}$), the HHV of solids was lower (2.0–6.1 MJ/kg_{dry}) compared to that of the digestate (11.1 MJ/kg_{dry}), resulting in a limited amount of residual embedded energy (7–27%). The van Krevelen diagrams (Figs. S7A-B) indicate a higher occurrence of dehydration and deamination reactions compared to biocrudes. Additionally, trends with solid loading were observed for the H/C and N/C ratios, and in both cases, these differed from those observed in biocrudes. Specifically, for H/C, the trend was opposite to that of biocrudes, while the N/C ratio increased with higher solid loading. These trends were statistically significant and the analysis of variance is reported in Table S8-9, while the resulting equations are provided in Eq. (S6) and Eq. (S7). A possible explanation for the N/C trend is described in Section 3.3, while the decreased H/C with increasing solid loading could be attributed to enhanced dehydration reactions between molecules, ultimately leading to the formation of a higher solid phase.

3.3. Carbon and nitrogen yields

Compared to analyzing mass yields, examining yields on a carbon and nitrogen basis is more valuable, as the goal of energy valorization is to maximize carbon and minimize nitrogen in the biocrude. Carbon contributes to the calorific value, while nitrogen poses significant challenges in the subsequent oil upgrading steps [66].

The response surface for the carbon yield is reported in Fig. 4, while the experimental values obtained for each experiment are reported in Fig. S8A. The biocrude phase had the highest carbon yield, with predicted values between 31% and 41%. The trend with temperature, dry solid loading, and time (Figs. 4A-B-C) were the same observed for the mass yields, but the carbon-based values were higher due to the higher carbon concentration in the biocrude compared to the digestate. For short residence times, the carbon yield for the solid phase (Figs. 4D-E-F) largely depended on the temperature, with lower temperatures (300 °C) leaving 27–28% of the carbon in the solid. In contrast, at 360 °C, it was possible to reduce the solid up to 14–17%. With longer residence times, a further decrease in carbon yield was observed, especially with lower dry solid loading.

For the quantification of the gas phase, it was assumed that it was composed only of CO_2, as justified in Section 3.4.1. In any case, its carbon yield was limited to 7–14%. Finally, the aqueous phase had the lowest carbon yield (2–13%), with lower dry solid loading strongly favoring higher yields (Figs. 4J-K-L). This can be attributed to the decreased solid-to-water ratio at lower solid loadings, which enhances the conversion of solids by water while effectively solubilizing and stabilizing the intermediates formed.

The contour plots for the nitrogen yield are shown in Fig. 5, while the experimental values obtained for each experiment are reported in Fig. S8B. Unlike carbon yield, the highest nitrogen yields were typically recorded in the AP. This is because nitrogen is more polar, increasing the solubility of nitrogen-containing molecules in the AP. Specifically, nitrogen yields were substantially high (37–41%) at the lowest dry solid loadings and drastically decreased with increasing solid loading (Figs. 5G-H-I). The nitrogen yield in the biocrude was also significant (13–33%, Figs. 5A-B-C). Interestingly, a maximum value was observed for intermediate dry solid loadings (21%). This particular trend was also observed with the N/C in Fig. 3, and is due to the substantial decrease in nitrogen concentration in the biocrude at higher solid loadings, which counterbalances the slight increase in biocrude yield. This can be explained by the fact that at the lowest solid loading, nitrogen tends to be more easily hydrolyzed in the AP, due to high water-to-solid ratio. As the dry solid loading increases, more nitrogen tends to be transferred to the biocrude phase. However, as solid loading increases further, the amount of dry solid feedstock becomes excessive, causing nitrogen yield to shift toward the solid phase at the expense of biocrude and AP yields.

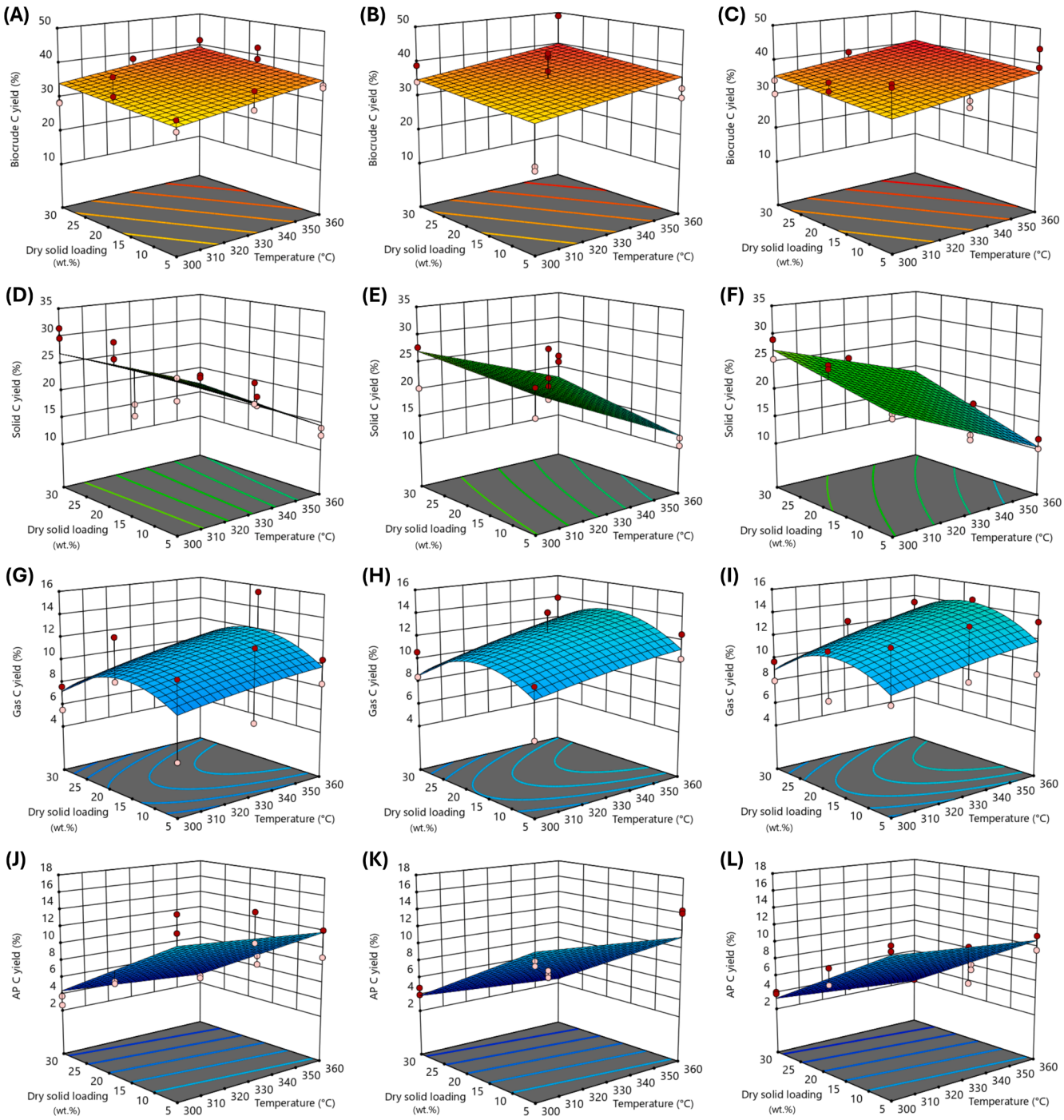

Fig. 4. Response surfaces for the carbon yields (%) obtained from HTL of digestate. Biocrude carbon yields after residence times of 10 min (A), 35 min (B), and 60 min (C). Solid carbon yields after residence times of 10 min (D), 35 min (E), and 60 min (F). Gas carbon yields after residence times of 10 min (G), 35 min (H), and 60 min (I). AP carbon yields after residence times of 10 min (J), 35 min (K), and 60 min (L).

Indeed, with increasing solid loading, nitrogen yields in the solid phase (Figs. 5D-E-F) rose significantly, from 6-14% (depending on temperature) to 12–21%.

The overall carbon balance from the experiments ranged from 54% to 74%, while the nitrogen balance ranged from 48% to 81%. The missing portions could be attributed to AP-solubles, as only approximately 50% of the initial distilled water was recovered as AP, along with biocrude losses during rotary evaporation and various losses during phases separation.

3.4. Composition of the phases

3.4.1. Gas phase

A sample of the gas phase produced at 360 °C for 60 min with a 30 wt % solid loading was analyzed. The resulting composition was 95.03 ± 3.75% CO_2, 1.72 ± 0.05% CH_4, 1.24 ± 0.15% CO, 0.93 ± 0.02% C_3H_8, 0.66 ± 0.04% H_2, 0.62 ± 0.08% C_2H_6 on a dry-volume basis. Since CO_2 concentration typically decreases with increasing reaction temperature [54], it is reasonable to assume that CO_2 levels were even higher at the lower temperature tested. This finding supports the common assumption that the gas phase consists primarily of CO_2, which was used above to

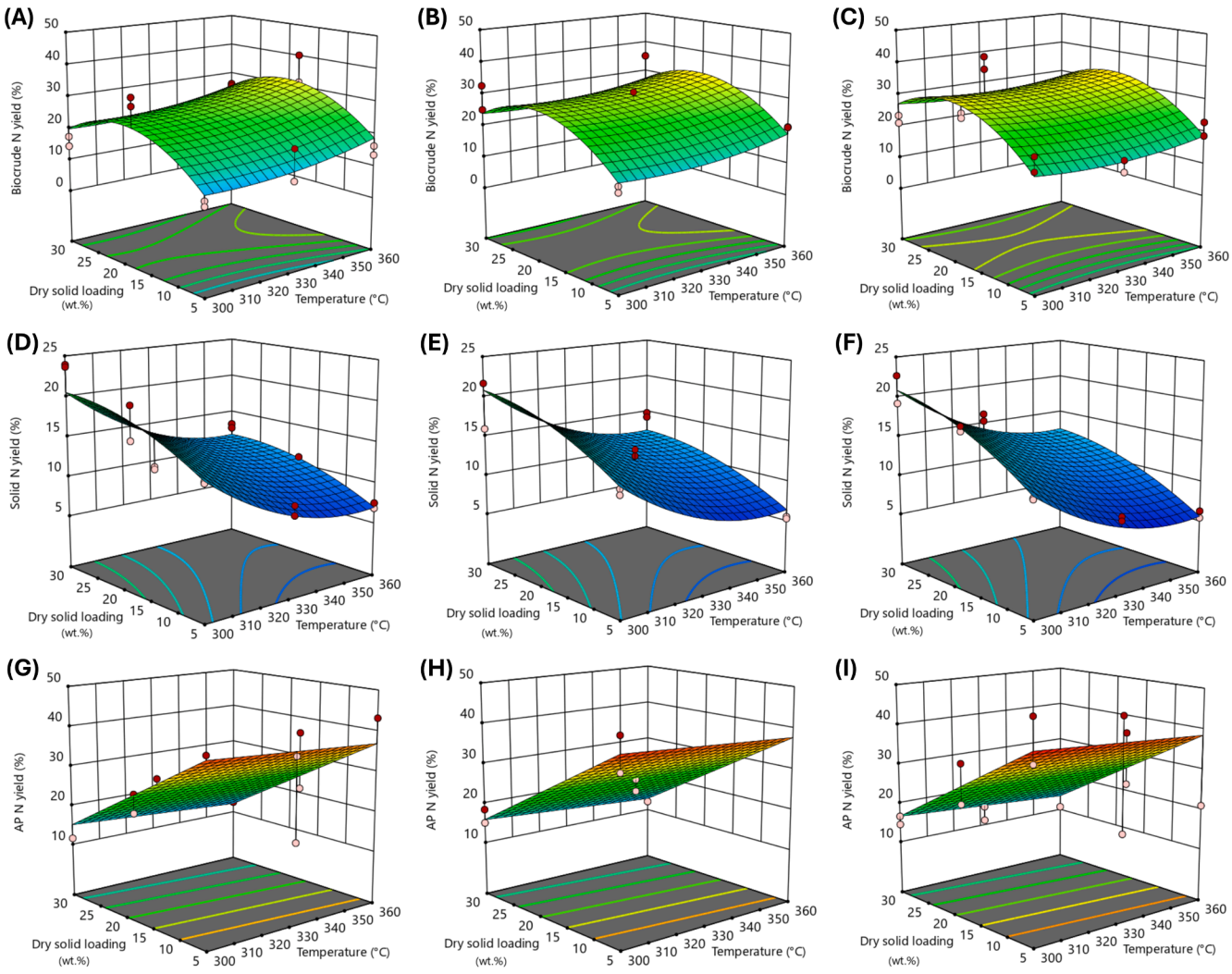

Fig. 5. Response surfaces for the nitrogen yields (%) obtained from HTL of digestate. Biocrude nitrogen yields after residence times of 10 min (A), 35 min (B), and 60 min (C). Solid nitrogen yields after residence times of 10 min (D), 35 min (E), and 60 min (F). AP nitrogen yields after residence times of 10 min (G), 35 min (H), and 60 min (I).

estimate the carbon yield of the gas phase.

To investigate the presence of trace compounds in the gas phase, GC–MS analysis was also performed, and the resulting list is reported in Table S10. Most compounds were saturated and unsaturated aliphatics, with a small fraction containing sulfur or nitrogen.

3.4.2. *Biocrude phase*

Fig. 6 illustrates the composition of the biocrudes, with the most prominent compounds listed in Table S11.

A significant quantity of sterols was detected in all biocrudes, consistent with previous findings from the HTL of digestate sewage sludge [25]. Sterols are polycyclic compounds that are not formed during HTL but are likely present in the feedstock, remaining relatively stable under hydrothermal conditions [67,68]. As apolar compounds, sterols may be found in waste originating from plants or animals, in the form of phytosterols or cholesterol, respectively. These compounds are not broken down during anaerobic digestion, thus persisting in the digestate [69]. A similar trend was observed for tocopherols, which are common in human food and likely present in the OFMSW [70], remaining unaltered through both AD and HTL. Both sterols and tocopherols showed a reduction in relative area as temperature and residence time increased. The decrease with temperature may be attributed to a higher concentration of other compounds, as evidenced by the increased biocrude yield at higher temperatures, leading to a lower relative concentration of sterols and tocopherols. However, the sharp decline with increased residence time cannot be explained by changes in biocrude yield, which remained relatively stable, but may be due to the slow degradation of these compounds during HTL [68].

The relative concentration of alkanes was also among the highest, indicating the high quality of the biocrude. Most of them were normal paraffins (Fig. S9A), followed by methyl-, dimethyl-, trimethyl-, and tetramethyl-substituted paraffins, in decreasing order of abundance. The amount of cyclic paraffins was significantly lower. The carbon number of paraffins ranged between 8 and 31, with most falling within the ranges of C13-C15, C20-C21, or C24-C29 (Fig. S9B). The first group (C13-C15) could be attributed to the decarboxylation of fatty acids [71], while longer hydrocarbons must have been formed through other mechanisms [72]. Alkenes were present in much lower quantities compared to alkanes (Fig. 6), and the majority of them consisted of 1-monoalkenes.

A significant amount of benzene-based molecules (phenols, guaiacols, and other phenolic structures) were identified. Guaiacols are derived from one of the three types of monomeric structures (coniferyl alcohol) present in the lignin fraction [73]. The most prominent guaiacols identified were guaiacol, 4-propylguaiacol, and 4-ethylguaiacol. Interestingly, the concentration of guaiacols decreased significantly with increasing temperatures, while an increase in phenols was observed. The most abundant phenols included phenol, cresol, and 4-

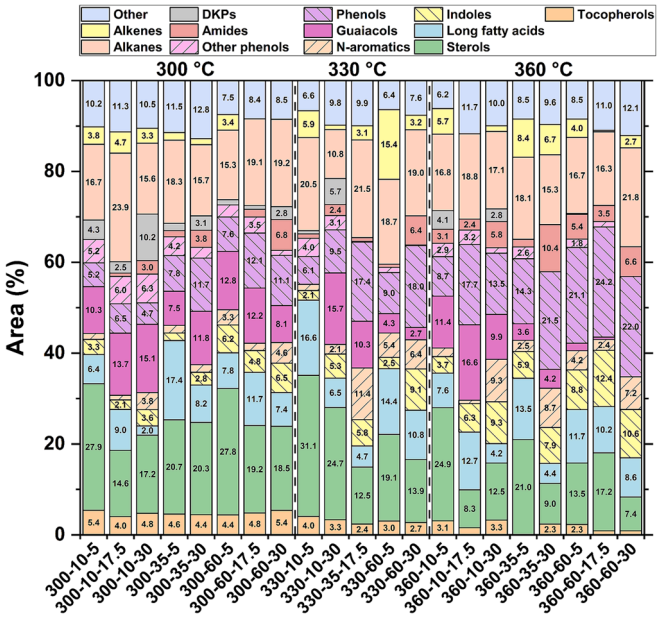

Fig. 6. Families of compounds identified after GC–MS of the biocrudes. DKPs refer to diketopiperazines. 'Other phenols' refers to 5-*tert*-butylpyrogallol and dimethoxyphenols.

ethylphenol, suggesting the conversion of guaiacols into their corresponding phenols through ether bond cleavage at higher temperatures [74].

Several nitrogen-containing aromatics were also detected, particularly indoles. In Fig. 6, the category 'N-aromatics' includes pyrazines, pyridoindole, quinolines, and pyrroles. These compounds originate from proteins and their interactions with carbohydrates and require higher temperatures to form [75], as indicated by their increased abundance at elevated temperatures. Other nitrogen-containing molecules included diketopiperazines (DKPs) and amides. DKPs are generated from the cyclization of amino acids [76] while amides consisted mostly of cyclic lactams, particularly pyrrolidinones (five-membered lactams), derived from proteins [77], and a few fatty amides, derived from the interaction of fatty acids with amino acids derivatives [78]. Amides showed an increased amount with higher dry solid loading. Nitrogen-containing compounds in biocrude have been reported as problematic, as their complete removal, essential for fuel production, is difficult to achieve through hydrodenitrogenation (HDN) [66]. Heterocyclic nitrogen, particularly in aromatic forms, is especially resistant to removal [66,79,80]. As shown in Fig. 6, increasing the temperature results in a higher ratio of nitrogen aromatics ('N-aromatics' and 'indoles') to aliphatic nitrogen ('DKPs' and 'amides'), likely due to the higher thermal stability of the former, making subsequent upgrading more challenging.

Overall, temperature is the most influential parameter affecting biocrude composition. At higher temperatures, lower concentrations of sterols and tocopherols were observed—polycyclic compounds that, if not fully hydrogenated during upgrading, could lead to cyclic hydrocarbons in the final fuel. Additionally, as temperature increased, the guaiacols-to-phenols ratio decreased; however, this had minimal impact on the final fuel, as guaiacols are converted into phenols during upgrading [81]. While higher temperatures benefited the aforementioned parameters, they also led to an increased aromatic-to-aliphatic nitrogen ratio, posing a significant challenge for removal during subsequent upgrading. Ultimately, overall aromatic content is primarily influenced by residence time, with shorter residence times reducing aromatics. A higher aromatic content in biocrude results in a more aromatic final fuel, which may be advantageous for specific applications, such as jet fuel. Moreover, longer residence time also favored decreased sterols and tocopherols, improving the fuel property.

In conclusion, while higher temperatures slightly enhance biocrude production and carbon recovery, they may also lead to a composition that is more challenging to upgrade, requiring a careful trade-off. As for residence time, its impact on biocrude yield is limited, but optimizing it can help achieve the desired aromatic content.

3.4.3. Aqueous phase

The composition of the aqueous phase was analyzed using GC–MS. The most abundant peaks are listed in Table S12, while the grouping in molecular families is depicted in Fig. 7. A significant portion of the peaks (46% of the total integrated area) corresponded to amines, predominantly short-chain aliphatic amines such as ethylamine, butylamine, isopentylamine, and propylamine. Phenethylamine was the only aromatic amine identified. In addition, lactams and amino acids were detected as other nitrogen-containing molecules. Lactams, particularly pyrrolidinones, as observed in the biocrude, were notably abundant. Amino acids result from the hydrolysis of the polypeptides that make up proteins, while lactams may form from the internal lactamization of amino acids [51,75]. Specifically, pyrrolidinones have been observed during HTL of glutamic acid [77], and ethylamine can derive from the decarboxylation of alanine [82,83], whereas the formation of longer amines like butylamine, isopentylamine, and propylamine cannot be easily attributed to simple amino acid decarboxylation. In fact, these amines are often not identified during HTL, likely due to their high polarity, which causes them to remain in the aqueous phase, a phase that is frequently under-characterized. Indeed, they have been observed in the water extract from biocrude HTL [84].

Characterizing nitrogen-containing compounds is crucial from an environmental perspective, as part of the aqueous phase post-HTL needs to be recycled to dilute the input for anaerobic digestion. However, these compounds can reduce the biomethane potential, along with the other nitrogen heterocycles identified in this work, namely pyrazines, and -piperidines [85–87].

In the aqueous phase, cyclopentenones, phenols, and both aliphatic and aromatic carboxylic acids were substantially identified. Cyclopentenones were present in very low concentrations in the biocrude, indicating a stronger tendency to remain in the aqueous phase. Phenols, however, were found in both the biocrude and aqueous phase, likely due to their intermediate solubility. Despite the substantial presence of

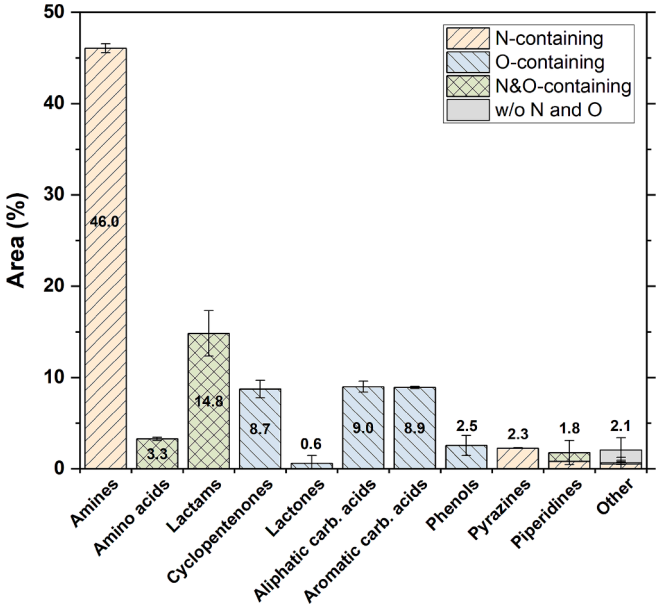

Fig. 7. Type of molecules identified via GC–MS in the aqueous phase obtained at 360 °C at 60 min and 5 wt%.

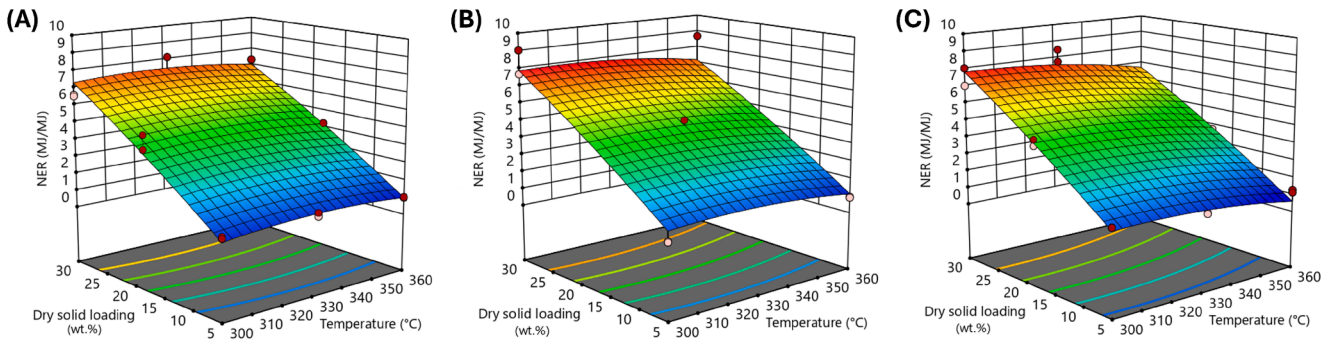

Fig. 8. Contour plots for the net energy recovery (MJ/MJ) as biocrude obtained from HTL of digestate after residence times of 10 min (A), 35 min (B), 60 min (C).

carboxylic acids, only 3-methylvaleric and isocaproic acids were identified as volatile fatty acids (VFAs). The other aliphatic carboxylic acids were C4-C6 acids with a higher boiling point and were either dicarboxylic (succinic, glutaric, and azelaic acid) or hydroxylated (4-hydroxybutyric acid, levulinic acid). Among the aromatic carboxylic acids, terephthalic, hydrocinnamic, benzoic, and p-hydroxybenzoic acid were the most prevalent.

3.5. Overall considerations

The HTL step allowed to convert digestate into biocrude, along with a CO_2-rich gas, residual solid, and aqueous phase. At 360 °C for 60 min and 30 wt% solids, the biocrude phase could reach the mass yield of 32%$_{daf}$, while retaining 41% of the carbon and 48% of the energy of the starting digestate. The net energy recovery (NER) in these conditions was equal to 6.7 (Fig. 8), confirming the energy profitability of the HTL of digestate. It is worth noting that besides slightly favoring the yields of biocrude, increasing the solid loading almost linearly favor the NER, as seen in Fig. 8. This is because while the heating demand remains fixed, biocrude production strongly depends on the dry solid loading.

The biocrude produced can be sold and used as feed for fuel production after proper upgrading, representing a key economic benefit of the process. Simultaneously, the HTL step reduces the amount of solid digestate, resulting in a residual solid of 35–37% of the dry digestate mass at 360 °C. This solid is more concentrated in ash (up to 80–88% at 360 °C) compared to untreated digestate (42%). Due to its high ash content and low HHV, further thermochemical conversion via combustion is not favorable. Additional evaluations are needed to assess the properties and potential applications of the solid hydrochar, including nutrient recovery, use as an adsorbent, or agricultural applications [88,89]. If no suitable applications are found, the residual solid must be disposed of; however, the HTL step would still reduce both the disposal volume and costs compared to untreated digestate. From an economic perspective, higher temperatures are preferable, as they enhance biocrude yield while reducing solid waste. However, higher temperatures and pressures are associated with more challenging conditions, both for the materials used for the reactor and the mechanical risks related to possible failures. These aspects, commonly not investigated due to the actual low TRL, should be addressed for the safe development of this novel process.

Although higher dry solid loading showed a slight increase in solid production (Fig. 2), especially at higher temperatures, it represented the optimal working conditions due to the higher energy profitability of the process (Fig. 8). Increasing the dry solid loading also provides the benefit of minimizing the solubilization of carbon and nitrogen in the aqueous phase. The valorization of the aqueous phase is crucial, as its disposal would negatively impact both economic and environmental performance. A primary process optimization strategy involves recirculating the aqueous phase at the inlet of the anaerobic digestion (AD) process. This approach can simultaneously reduce freshwater demand for AD and lower the organic loading of the stream.

To the best of the authors' knowledge, the effects of amines and lactams – the predominant compounds identified in the aqueous phase – on anaerobic digestion (AD) have not yet been investigated. Amines can be converted into ammonia, which, in excessive concentrations, is known to inhibit AD. However, this inhibition should be experimentally assessed, as microbial consortium acclimation may mitigate its impact [90]. Regarding lactams, certain antibiotics classified as β-lactams, characterized by a four-membered lactam ring (hence the name β-lactams), have been reported to inhibit methane production during the AD of waste [91]. However, given the structural differences between these antibiotics and pyrrolidinones – the five-membered γ-lactams observed in this study – this inhibitory effect requires experimental validation.

Further research is essential to assess the impact of aqueous phase recirculation and to optimize it.

4. Conclusions

The performance of hydrothermal liquefaction (HTL) of digestate derived from the organic fraction of municipal solid waste (OFMSW) was investigated by varying operating temperature (300–360 °C), residence time (10–60 min), and dry solid loading (5–30 wt%). Higher temperatures were found optimal for minimizing residual solids (down to 7 wt%), maximizing biocrude yield (up to 32 wt%), and enhancing its aromatic content, which made nitrogen removal more difficult during the subsequent upgrading step. Increasing the dry solid loading resulted in a rise in residual solids (up to 24 wt%) at the expense of aqueous phase (AP) soluble compounds (with a minimum 4% carbon yield), and altered the elemental ratios of biocrudes and solids. The AP was notably rich in amines and lactams, while the biocrude contained high concentrations of sterols, n-paraffins, phenols, and guaiacols. This study demonstrates the effectiveness of HTL in converting digestate into an energy-dense biocrude (~31 MJ/kg), suitable for fuel production. HTL also shows potential advantages over the thermochemical alternative of digestate pyrolysis. These findings lay the groundwork for energetically, economically, and environmentally integrating anaerobic digestion and HTL, which should be further explored in future research.

CRediT authorship contribution statement

Edoardo Tito: Writing – review & editing, Writing – original draft, Visualization, Validation, Methodology, Investigation, Formal analysis, Data curation, Conceptualization. **Daniela Landi:** Investigation, Data curation. **Francesca Demichelis:** Writing – review & editing, Validation, Supervision, Methodology, Conceptualization. **Giuseppe Pipitone:** Writing – review & editing, Validation, Supervision, Methodology, Conceptualization. **Samir Bensaid:** Writing – review & editing, Supervision, Project administration, Funding acquisition, Conceptualization. **Raffaele Pirone:** Writing – review & editing, Validation, Project administration, Funding acquisition, Conceptualization.

Declaration of competing interest

The authors declare that they have no known competing financial interests or personal relationships that could have appeared to influence the work reported in this paper.

Acknowledgments

Edoardo Tito gratefully acknowledges the ReFuel project – funded by European Union – Next Generation EU within the PRIN 2022 program (D.D. 104 - 02/02/2022 Ministero dell'Università e della Ricerca).

The authors thank Acea Pinerolese Energia S.r.l. for providing the digestate used in this work.

Appendix A. Supplementary data

Supplementary data to this article can be found online at https://doi.org/10.1016/j.enconman.2025.119881.

Data availability

Data will be made available on request.

References

[1] Energy Institute. Statistical Review of World Energy. Smil (2017) – with major processing by Our World in Data. "Primary energy from biofuels"; 2024.
[2] United Nations Environment Programme. Beyond an age of waste - global waste management outlook 2024; 2024. doi:10.59117/20.500.11822/44939.
[3] Pham TPT, Kaushik R, Parshetti GK, Mahmood R, Balasubramanian R. Food waste-to-energy conversion technologies: Current status and future directions. Waste Manag 2015;38:399–408. https://doi.org/10.1016/j.wasman.2014.12.004.
[4] Tyagi VK, Fdez-Güelfo LA, Zhou Y, Álvarez-Gallego CJ, Garcia LIR, Ng WJ. Anaerobic co-digestion of organic fraction of municipal solid waste (OFMSW): progress and challenges. Renew Sustain Energy Rev 2018;93:380–99. https://doi.org/10.1016/j.rser.2018.05.051.
[5] Babu R, Prieto Veramendi PM, Rene ER. Strategies for resource recovery from the organic fraction of municipal solid waste. Case Stud Chem Environ Eng 2021;3:100098. https://doi.org/10.1016/j.cscee.2021.100098.
[6] Issah AA, Kabera T, Kemausuor F. Biogas optimisation processes and effluent quality: a review. Biomass Bioenergy 2020;133:105449. https://doi.org/10.1016/j.biombioe.2019.105449.
[7] da Cunha AP, Cammarota MC, Volschan Jr I. Anaerobic co-digestion of sewage sludge and food waste: effect of pre-fermentation of food waste in bench- and pilot-scale digesters. Bioresour Technol Reports 2021;15:100707. https://doi.org/10.1016/j.biteb.2021.100707.
[8] Van DP, Fujiwara T, Leu Tho B, Song Toan PP, Hoang MG. A review of anaerobic digestion systems for biodegradable waste: Configurations, operating parameters, and current trends. Environ Eng Res 2019;25:1–17. https://doi.org/10.4491/eer.2018.334.
[9] Czekała W, Nowak M, Piechota G. Sustainable management and recycling of anaerobic digestate solid fraction by composting: A review. Bioresour Technol 2023:375. https://doi.org/10.1016/j.biortech.2023.128813.
[10] Wang W, Lee DJ. Valorization of anaerobic digestion digestate: A prospect review. Bioresour Technol 2021;323:124626. https://doi.org/10.1016/j.biortech.2020.124626.
[11] European Commission. Commission Regulation (EU) 2019/1691. 2019.
[12] Tampio E, Salo T, Rintala J. Agronomic characteristics of five different urban waste digestates. J Environ Manage 2016;169:293–302. https://doi.org/10.1016/j.jenvman.2016.01.001.
[13] European Commission. Commission Regulation (EU) 2019/1009; 2019.
[14] Dahlin J, Herbes C, Nelles M. Biogas digestate marketing: Qualitative insights into the supply side. Resour Conserv Recycl 2015;104:152–61. https://doi.org/10.1016/j.resconrec.2015.08.013.
[15] Dutta S, He M, Xiong X, Tsang DCW. Sustainable management and recycling of food waste anaerobic digestate: A review. Bioresour Technol 2021;341:125915. https://doi.org/10.1016/j.biortech.2021.125915.
[16] Wang W, Chang J-S, Lee D-J. Anaerobic digestate valorization beyond agricultural application: Current status and prospects. Bioresour Technol 2023;373:128742. https://doi.org/10.1016/j.biortech.2023.128742.
[17] Mathanker A, Das S, Pudasainee D, Khan M, Kumar A, Gupta R. A review of hydrothermal liquefaction of biomass for biofuels production with a special focus on the effect of process parameters, co-solvents and extraction solvents. Energies 2021;14:4916. https://doi.org/10.3390/en14164916.
[18] Mishra RK, Kumar V, Kumar P, Mohanty K. Hydrothermal liquefaction of biomass for bio-crude production: A review on feedstocks, chemical compositions, operating parameters, reaction kinetics, techno-economic study, and life cycle assessment. Fuel 2022;316:123377. https://doi.org/10.1016/j.fuel.2022.123377.
[19] Mahadevan V, Subbaiyan N, Kannappan Panchamoorthy G, Jayaseelan A, Palaniappan SK, Siengchin S. Hydrothermal liquefaction of confused waste to bio-oil: A study on elemental and energy recovery. Energy Convers Manag 2025;325:119353. https://doi.org/10.1016/j.enconman.2024.119353.
[20] Toor SS, Rosendahl L, Rudolf A, Sohail S, Rosendahl L, Rudolf A. Hydrothermal liquefaction of biomass: A review of subcritical water technologies. Energy 2011;36:2328–42. https://doi.org/10.1016/j.energy.2011.03.013.
[21] Akiya N, Savage PE. Roles of water for chemical reactions in high-temperature water. Chem Rev 2002;102:2725–50. https://doi.org/10.1021/cr000668w.
[22] Silva Thomsen LB, Anastasakis K, Biller P. Hydrothermal liquefaction potential of wastewater treatment sludges: Effect of wastewater treatment plant and sludge nature on products distribution. Fuel 2024:355. https://doi.org/10.1016/j.fuel.2023.129525.
[23] Hegdahl SH, Ghoreishi S, Løhre C, Barth T. Exploring hydrothermal liquefaction (HTL) of digested sewage sludge (DSS) at 5.3 L and 0.025 L bench scale using experimental design. Sci Rep 2023;13:18806. https://doi.org/10.1038/s41598-023-45957-9.
[24] Aragon-Briceño CI, Ross AB, Camargo-Valero MA. Strategies for the Revalorization of Sewage Sludge in a Waste Water Treatment Plant Through the Integration of Hydrothermal Processing. Waste Biomass Valoriz 2023;14:105–26. https://doi.org/10.1007/s12649-022-01856-0.
[25] Hegdahl SH, Løhre C, Barth T. Hydrothermal liquefaction of sewage sludge anaerobic digestate for bio-oil production: Screening the effects of temperature, residence time and KOH catalyst. Waste Manag Res 2022. https://doi.org/10.1177/0734242X221138497.
[26] Vardon DR, Sharma BK, Scott J, Yu G, Wang Z, Schideman L, et al. Chemical properties of biocrude oil from the hydrothermal liquefaction of Spirulina algae, swine manure, and digested anaerobic sludge. Bioresour Technol 2011;102:8295–303. https://doi.org/10.1016/j.biortech.2011.06.041.
[27] Ekpo U, Ross AB, Camargo-Valero MA, Williams PT. A comparison of product yields and inorganic content in process streams following thermal hydrolysis and hydrothermal processing of microalgae, manure and digestate. Bioresour Technol 2016;200:951–60. https://doi.org/10.1016/j.biortech.2015.11.018.
[28] Aragon-Briceño C, Ross AB, Camargo-Valero MA. Evaluation and comparison of product yields and bio-methane potential in sewage digestate following hydrothermal treatment. Appl Energy 2017;208:1357–69. https://doi.org/10.1016/j.apenergy.2017.09.019.
[29] Okoro OV, Sun Z, Birch J. Thermal depolymerization of biogas digestate as a viable digestate processing and resource recovery strategy. Elsevier Ltd; 2018. https://doi.org/10.1016/B978-0-08-102728-8.00010-3.
[30] Okoro OV, Sun Z, Birch J. Prognostic assessment of the viability of hydrothermal liquefaction as a post-resource recovery step after enhanced biomethane generation using co-digestion technologies. Appl Sci 2018;8:doi:10.3390/app8112290.
[31] Sudibyo H, Tester JW. Sustainable Resource Recovery from Dairy Waste: A Case Study of Hydrothermal Co-liquefaction of Acid Whey and Anaerobic Digestate Mixture. Energy Fuels 2023;37:2897–911. https://doi.org/10.1021/acs.energyfuels.2c03860.
[32] Eboibi BE, Lewis DM, Ashman PJ, Chinnasamy S. Integrating anaerobic digestion and hydrothermal liquefaction for renewable energy production: an experimental investigation. Environ Prog Sustain Energy 2015;34:1662–73. https://doi.org/10.1002/ep.12172.
[33] Rao U, Posmanik R, Hatch LE, Tester JW, Walker SL, Barsanti KC, et al. Coupling hydrothermal liquefaction and membrane distillation to treat anaerobic digestate from food and dairy farm waste. Bioresour Technol 2018;267:408–15. https://doi.org/10.1016/j.biortech.2018.07.064.
[34] Posmanik R, Martinez CM, Cantero-Tubilla B, Cantero DA, Sills DL, Cocero MJ, et al. Acid and alkali catalyzed hydrothermal liquefaction of dairy manure digestate and food waste. ACS Sustain Chem Eng 2018;6:2724–32. https://doi.org/10.1021/acssuschemeng.7b04359.
[35] Klüpfel C, Herklotz B, Biller P. Influence of processing conditions and biochemical composition on the hydrothermal liquefaction of digested urban and agricultural wastes. Fuel 2023;352:129016. https://doi.org/10.1016/j.fuel.2023.129016.
[36] Klüpfel C, Yuan B, Biller P, Herklotz B. Hydrothermal liquefaction as a treatment technology for anaerobic digestate: A review. Renew Sustain Energy Rev 2025;210:115156. https://doi.org/10.1016/j.rser.2024.115156.
[37] Biller P, Ross AB. Production of biofuels via hydrothermal conversion. Handb Biofuels Prod Process Technol Second Ed 2016:509–47. https://doi.org/10.1016/B978-0-08-100455-5.00017-5.
[38] Adekunle KF, Okolie JA. A Review of Biochemical Process of Anaerobic Digestion 2015:205–12.
[39] Zhang C, Shao M, Wu H, Wang N, Wang X, Wang Q, et al. Mechanism insights into hydrothermal dewatering of food waste digestate for products valorization. Sci Total Environ 2022;804:150145. https://doi.org/10.1016/j.scitotenv.2021.150145.
[40] Sheets JP, Yang L, Ge X, Wang Z, Li Y. Beyond land application: Emerging technologies for the treatment and reuse of anaerobically digested agricultural and food waste. Waste Manag 2015;44:94–115. https://doi.org/10.1016/j.wasman.2015.07.037.
[41] Tito E, Zoppi G, Pipitone G, Miliotti E, Di FA, Rizzo AM, et al. Conceptual design and techno-economic assessment of coupled hydrothermal liquefaction and aqueous phase reforming of lignocellulosic residues. J Environ Chem Eng 2023;11:109076. https://doi.org/10.1016/j.jece.2022.109076.
[42] Snowden-Swan LJ, Hallen RT, Billing JM, Zhu Y, Hart TR, Jones SB, et al. Hydrothermal liquefaction and upgrading of municipal wastewater treatment plant

sludge: a preliminary techno-economic analysis. United States Department of Energy, PNNL report; 2016.
[43] Tito E, Marcolongo CA, Pipitone G, Monteverde AHA, Bensaid S, Pirone R. Understanding the effect of heating rate on hydrothermal liquefaction: a comprehensive investigation from model compounds to a real food waste. Bioresour Technol 2024;396:130446. https://doi.org/10.1016/j.biortech.2024.130446.
[44] Simonne AH, Simonne EH, Eitenmiller RR, Mills HA, Cresman CP. Could the dumas method replace the Kjeldahl digestion for nitrogen and crude protein determinations in foods? J Sci Food Agric 1997;73:39–45. https://doi.org/10.1002/(SICI)1097-0010(199701)73:1<39::AID-JSFA717>3.3.CO;2-W.
[45] TAPPI. Reaffirmation of T 222 om-02. n.d.
[46] Channiwala SA, Parikh PP. A unified correlation for estimating HHV of solid, liquid and gaseous fuels. Fuel 2002;81:1051–63. https://doi.org/10.1016/S0016-2361(01)00131-4.
[47] Jones S, Zhu Y, Anderson D, Hallen RT, Elliott DC. Process design and economics for the conversion of algal biomass to hydrocarbons: whole algae hydrothermal liquefaction and upgrading. PNNL 2014:1–69.
[48] Madsen RB, Jensen MM, Mørup AJ, Houlberg K, Christensen PS, Klemmer M, et al. Using design of experiments to optimize derivatization with methyl chloroformate for quantitative analysis of the aqueous phase from hydrothermal liquefaction of biomass. Anal Bioanal Chem 2016;408:2171–83. https://doi.org/10.1007/s00216-016-9321-6.
[49] Madsen RB, Christensen PS, Houlberg K, Lappa E, Mørup AJ, Klemmer M, et al. Analysis of organic gas phase compounds formed by hydrothermal liquefaction of Dried Distillers Grains with Solubles. Bioresour Technol 2015;192:826–30. https://doi.org/10.1016/j.biortech.2015.05.095.
[50] Biller P, Ross AB. Potential yields and properties of oil from the hydrothermal liquefaction of microalgae with different biochemical content. Bioresour Technol 2011;102:215–25. https://doi.org/10.1016/j.biortech.2010.06.028.
[51] Changi SM, Faeth JL, Mo N, Savage PE. Hydrothermal reactions of biomolecules relevant for microalgae liquefaction. Ind Eng Chem Res 2015;54:11733–58. https://doi.org/10.1021/acs.iecr.5b02771.
[52] Peterson AA, Vogel F, Lachance RP, Fröling M, Antal Jr MJ, Tester JW. Thermochemical biofuel production in hydrothermal media: a review of sub- and supercritical water technologies. Energy Environ Sci 2008;1:32. https://doi.org/10.1039/b810100k.
[53] Madsen RB, Glasius M. How do hydrothermal liquefaction conditions and feedstock type influence product distribution and elemental composition? Ind Eng Chem Res 2019;58:17583–600. https://doi.org/10.1021/acs.iecr.9b02337.
[54] Tito E, Pipitone G, Monteverde Videla AHA, Bensaid S, Pirone R. Exploring HTL pathways in carbohydrate–protein mixture: a study on glucose–glycine interaction. Biomass Convers Biorefin 2023;13:16385–404. https://doi.org/10.1007/s13399-023-03967-7.
[55] Mathimani T, Mallick N. A review on the hydrothermal processing of microalgal biomass to bio-oil - Knowledge gaps and recent advances. J Clean Prod 2019;217:69–84. https://doi.org/10.1016/j.jclepro.2019.01.129.
[56] Yi W, Zheng D, Wang X, Chen Y, Hu J, Yang H, et al. Biomass hydrothermal conversion under CO_2 atmosphere: a way to improve the regulation of hydrothermal products. Sci Total Environ 2022;807:150900. https://doi.org/10.1016/j.scitotenv.2021.150900.
[57] Singh R, Balagurumurthy B, Prakash A, Bhaskar T. Catalytic hydrothermal liquefaction of water hyacinth. Bioresour Technol 2015;178:157–65. https://doi.org/10.1016/j.biortech.2014.08.119.
[58] Liu HM, Li MF, Sun RC. Hydrothermal liquefaction of cornstalk: 7-Lump distribution and characterization of products. Bioresour Technol 2013;128:58–64. https://doi.org/10.1016/j.biortech.2012.09.125.
[59] Yin S, Dolan R, Harris M, Tan Z. Subcritical hydrothermal liquefaction of cattle manure to bio-oil: Effects of conversion parameters on bio-oil yield and characterization of bio-oil. Bioresour Technol 2010;101:3657–64. https://doi.org/10.1016/j.biortech.2009.12.058.
[60] Xu C, Lancaster J. Conversion of secondary pulp/paper sludge powder to liquid oil products for energy recovery by direct liquefaction in hot-compressed water. Water Res 2008;42:1571–82. https://doi.org/10.1016/j.watres.2007.11.007.
[61] Prestigiacomo C, Scialdone O, Galia A. Hydrothermal liquefaction of wet biomass in batch reactors: Critical assessment of the role of operating parameters as a function of the nature of the feedstock. J Supercrit Fluids 2022;189:105689. https://doi.org/10.1016/j.supflu.2022.105689.
[62] Motavaf B, Savage PE. Effect of process variables on food waste valorization via hydrothermal liquefaction. ACS ES&T Eng 2021;1:363–74. https://doi.org/10.1021/acsestengg.0c00115.
[63] Opatokun SA, Strezov V, Kan T. Product based evaluation of pyrolysis of food waste and its digestate. Energy 2015;92:349–54. https://doi.org/10.1016/j.energy.2015.02.098.
[64] Fast PND. Pyrolysis as a thermal treatment for post- digested sludges of crop waste to recover energy. The University of Nottingham; 2016.
[65] Monlau F, Sambusiti C, Antoniou N, Barakat A, Zabaniotou A. A new concept for enhancing energy recovery from agricultural residues by coupling anaerobic digestion and pyrolysis process. Appl Energy 2015;148:32–8. https://doi.org/10.1016/j.apenergy.2015.03.024.
[66] Castello D, Haider MS, Rosendahl LA. Catalytic upgrading of hydrothermal liquefaction biocrudes: different challenges for different feedstocks. Renew Energy 2019;141:420–30. https://doi.org/10.1016/j.renene.2019.04.003.
[67] Cabrera DV, Barria DA, Camu E, Celis C, Tester JW, Labatut RA. Enhancing energy recovery of wastewater treatment plants through hydrothermal liquefaction. Environ Sci Water Res Technol 2022;9:474–88. https://doi.org/10.1039/d2ew00752e.
[68] Hietala DC, Savage PE. Reaction pathways and kinetics of cholesterol in high-temperature water. Chem Eng J 2015;265:129–37. https://doi.org/10.1016/j.cej.2014.12.020.
[69] Weckerle T, Ewald H, Guth P, Knorr KH, Philipp B, Holert J. Biogas digestate as a sustainable phytosterol source for biotechnological cascade valorization. Microb Biotechnol 2023;16:337–49. https://doi.org/10.1111/1751-7915.14174.
[70] Yadav S, Malik K, Moore JMC, Kamboj BR, Malik S, Malik VK, et al. Valorisation of agri-food waste for bioactive compounds: recent trends and future sustainable challenges. Molecules 2024;29:1–23. https://doi.org/10.3390/molecules29092055.
[71] Obeid R, Lewis DM, Smith N, Hall T, van Eyk P, Van EP. Reaction kinetics and characterisation of species in renewable crude from hydrothermal liquefaction of monomers to represent organic fractions of biomass feedstocks. Chem Eng J 2020;389:124397. https://doi.org/10.1016/j.cej.2020.124397.
[72] Yue Y, Kastner JR, Mani S. Two-stage hydrothermal liquefaction of sweet sorghum biomass - part II: production of upgraded biocrude oil. Energy Fuels 2018;32:7620–9. https://doi.org/10.1021/acs.energyfuels.8b00669.
[73] Dunn KG, Hobson PA. Hydrothermal liquefaction of lignin. Sugarcane-Based Biofuels Bioprod 2016:165–206. https://doi.org/10.1002/9781118719862.ch7.
[74] Yong TLK, Yukihiko M. Kinetic analysis of guaiacol conversion in sub- and supercritical water. Ind Eng Chem Res 2013;52:9048–59. https://doi.org/10.1021/ie4009748.
[75] Fan Y, Hornung U, Dahmen N, Kruse A. Hydrothermal liquefaction of protein-containing biomass: study of model compounds for Maillard reactions. Biomass Convers Biorefin 2018;8:909–23. https://doi.org/10.1007/s13399-018-0340-8.
[76] Sakata K, Kitadai N, Yokoyama T. Effects of pH and temperature on dimerization rate of glycine: Evaluation of favorable environmental conditions for chemical evolution of life. Geochim Cosmochim Acta 2010;74:6841–51. https://doi.org/10.1016/j.gca.2010.08.032.
[77] Déniel M, Haarlemmer G, Roubaud A, Weiss-Hortala E, Fages J. Hydrothermal liquefaction of blackcurrant pomace and model molecules: understanding of reaction mechanisms. Sustain Energy Fuels 2017;1:555–82. https://doi.org/10.1039/C6SE00065G.
[78] Chiaberge S, Leonardis I, Fiorani T, Bianchi G, Cesti P, Bosetti A, et al. Amides in bio-oil by hydrothermal liquefaction of organic wastes: A mass spectrometric study of the thermochemical reaction products of binary mixtures of amino acids and fatty acids. Energy Fuels 2013;27:5287–97. https://doi.org/10.1021/ef4009983.
[79] Girgis MJ, Gates BC, Girgis MJ. Reactivities, Reaction Networks, and Kinetics in High-Pressure Catalytic Hydroprocessing. Ind Eng Chem Res 1991;30:2021–58. https://doi.org/10.1021/ie00057a001.
[80] Zimmermann J, Raffelt K, Dahmen N. Suppressing the formation of N-heteroaromatics during hydrothermal liquefaction of proteinaceous model feedstock. Biomass Convers Biorefin 2023;14:24671–83. https://doi.org/10.1007/s13399-023-04553-7.
[81] Heracleous E, Vassou M, Lappas AA, Rodriguez JK, Chiaberge S, Bianchi D. Understanding the upgrading of sewage sludge-derived hydrothermal liquefaction biocrude via advanced characterization. Energy Fuels 2022;36:12010–20. https://doi.org/10.1021/acs.energyfuels.2c01746.
[82] Bada JL, Miller SL, Zhao M. The stability of amino acids at submarine hydrothermal vent temperatures. Orig Life Evol Biosph 1995;25:111–8. https://doi.org/10.1007/BF01581577.
[83] Klingler D, Berg J, Vogel H. Hydrothermal reactions of alanine and glycine in sub- and supercritical water. J Supercrit Fluids 2007;43:112–9. https://doi.org/10.1016/j.supflu.2007.04.008.
[84] Chen WT, Tang L, Qian W, Scheppe K, Nair K, Wu Z, et al. Extract nitrogen-containing compounds in biocrude oil converted from wet biowaste via hydrothermal liquefaction. ACS Sustain Chem Eng 2016;4:2182–90. https://doi.org/10.1021/acssuschemeng.5b01645.
[85] Watson J, Wang T, Si B, Chen WT, Aierzhati A, Zhang Y. Valorization of hydrothermal liquefaction aqueous phase: pathways towards commercial viability. Prog Energy Combust Sci 2020;77:100819. https://doi.org/10.1016/j.pecs.2019.100819.

[86] Macêdo WV, Harpøth RD, Poulsen JS, de Jonge N, Fischer CH, Agneessens LM, et al. Anaerobic digestion of wastewater from hydrothermal liquefaction of sewage sludge and combined wheat straw-manure. Bioresour Technol 2024:399. https://doi.org/10.1016/j.biortech.2024.130559.

[87] Basar IA, Liu H, Eskicioglu C. Incorporating hydrothermal liquefaction into wastewater treatment – Part III: Aqueous phase characterization and evaluation of on-site treatment. Chem Eng J 2023;467:143422. https://doi.org/10.1016/j.cej.2023.143422.

[88] Liu H, Basar IA, Nzihou A, Eskicioglu C. Hydrochar derived from municipal sludge through hydrothermal processing: A critical review on its formation, characterization, and valorization. Water Res 2021;199:117186. https://doi.org/10.1016/j.watres.2021.117186.

[89] Liu H, Lyczko N, Nzihou A, Eskicioglu C. Incorporating hydrothermal liquefaction into wastewater treatment – Part II: Characterization, environmental impacts, and potential applications of hydrochar. J Clean Prod 2023;383:135398. https://doi.org/10.1016/j.jclepro.2022.135398.

[90] Puig-Castellví F, Cardona L, Bureau C, Bouveresse D-J-R, Cordella CBY, Mazéas L, et al. Effect of ammonia exposure and acclimation on the performance and the microbiome of anaerobic digestion. Bioresour Technol Reports 2020;11:100488. https://doi.org/10.1016/j.biteb.2020.100488.

[91] Xiao L, Wang Y, Lichtfouse E, Li Z, Kumar PS, Liu J, et al. Effect of antibiotics on the microbial efficiency of anaerobic digestion of wastewater: a review. Front Microbiol 2021;11:1–11. https://doi.org/10.3389/fmicb.2020.611613.